ELSEVIER

Chemical Engineering Journal 135 (2008) 224–231

Chemical Engineering Journal

www.elsevier.com/locate/cej

Liquid-wall mass transfer in three phase fluidized beds with cross-flow of electrolyte

K.V. Ramesh, G.M.J. Raju *, C. Bhaskara Sarma, R.V. Subba Raju

Department of Chemical Engineering, Andhra University, Visakhapatnam 530003, India

Received 7 March 2006; received in revised form 12 March 2007; accepted 19 March 2007

Abstract

Liquid-wall mass transfer coefficients were computed in a gas–liquid fluidized bed from the limiting current data obtained at the outer surface of different cross electrodes for both the cases of oxidation of ferrocyanide and reduction of ferricyanide ion. Particles of different sizes and densities were used as bed material and electrodes of five different diameters of length 44.5 mm were used. The fluid electrolyte velocities were varied from minimum fluidization velocities to well below the terminal velocities of the particles before the gas phase enters the test section. The liquid-wall mass transfer coefficient increased with increasing superficial gas velocity at a constant superficial liquid velocity upto a certain extent and reached a plateau. At constant superficial gas velocity, k_L increased with increasing superficial liquid velocity. k_L decreased with increase in electrode diameter. The effect of particle size on k_L was found to segregate into two regions, one for $d_p > 4$ mm and the other for $d_p < 4$ mm. k_L increased with increase in ε, reached a maximum and beyond an ε value of 0.85 showed a declining trend. The liquid-wall mass transfer coefficient data for both oxidation and reduction were correlated in terms of Coulburn factor j_D, void fraction ε, Reynolds number based on electrode diameter Re, Froude number based on gas velocity Fr_g and gas to liquid mass velocity ratio G_{mr}.

Keywords: Three phase fluidization; Cross-flow; Ionic mass transfer; Liquid-wall mass transfer; Mass transfer coefficient

1. Introduction

Three-phase fluidization [1–7] is considered to be one of the vital methods of multiphase flow contacting operation because many fold improvement in heat and mass transfer coefficients is observed in it in comparison with two-phase and homogeneous flow systems in general. Further, it provides intimate mixing, isothermal conditions, uniform concentrations, high heat and mass transfer rates, high liquid holdup, ability to use small catalyst particles, accurate temperature control to achieve good selectivity and increased protection of catalyst, etc. Hence it finds wide applications in petrochemical industries, chemical and allied industries, and in biochemical processing.

Its applications in petrochemical industries are for hydrogenation of liquid petroleum fractions, hydrodesulphurization of residual and heavy oils, benzene desulphurization, Fisher-Tropsch process, hydrocracking the oil to lighter fractions, coal conversion processes, coal liquefaction and pelletizing operations. In chemical and allied industries, it is found useful for catalytic hydrogenations and oxidations in particular hydrogenation of unsaturated fats, slurry methanation of carbon monoxide, production of calcium bisulphate cooking liquor in pulp and paper industry, synthesis gas conversion processes, turbulent contacting absorption of flue gas desulphurization and particulate removal, spray extraction columns and electrowinning. Further its applications can be adaptable for many biological and biochemical processes using immobilized whole cells, sub cellular organelles, or enzymes as the solid phase and for the processes like fermentation, cell cultivation, production of antibiotics and waste water treatment.

Studies on the mass transfer in three-phase fluidized beds are divided into two modes: gas–liquid mass transfer and liquid-wall mass transfer. The gas–liquid mass transfer is characterized by volumetric gas–liquid mass transfer coefficient and is investigated extensively [6]. Two kinds of investigations are made with respect to liquid-wall mass transfer: particle-to-liquid and wall-to-bed. Numerous investigations [6] have been carried out on particle-liquid mass transfer, as it is very important and significant in catalytic reactions. Application of three-phase fluidization to solid–liquid reactions or fluid–fluid reactions greatly

* Corresponding author. Tel.: +91 9866017067; fax: +91 891 2537793.
E-mail address: gmjraju@gmail.com (G.M.J. Raju).

1385-8947/$ – see front matter © 2007 Elsevier B.V. All rights reserved.
doi:10.1016/j.cej.2007.03.024

Nomenclature

A	surface area of the electrode (m^2)
C_0	concentration of ion at the surface of the electrode ($kmol/m^3$)
d_e	electrode diameter (m)
d_p	particle diameter (m)
D_c	column diameter (m)
D_L	diffusivity of transfer species (m^2/s)
F	Faraday constant, 96,500 (C/mol)
Fr_g	Froude number based on gas velocity, U_g^2/gD_c
g	acceleration due to gravity, 9.81 (m/s^2)
G_{mr}	mass velocity ratio, $U_g\rho_g/U_L\rho_L$
i_L	limiting current (A)
j_D	Colburn j-factor $(k_L/U_L)Sc^{2/3}$
k_L	liquid-wall mass transfer coefficient (m/s)
k_{LO}	mass transfer coefficient for oxidation (m/s)
Re	Reynolds number based on electrode diameter, $\rho_L d_e U_L/\mu_L$
Sc	Schmidt number, $\mu_L/\rho_L D_L$
U_g	superficial gas velocity (m/s)
U_L	superficial liquid velocity (m/s)
z	number of electrons per ion reacted at electrode surface

Greek letters

ε	bed porosity
μ_L	liquid viscosity (kg/m s)
ρ_g	gas density (kg/m^3)
ρ_L	liquid density (kg/m^3)
ρ_s	particle density (kg/m^3)

enhances the mass transfer rates due to creation of intense turbulence. The present study of liquid-wall mass transfer is that of wall-to-bed mass transfer, which plays a vital role in electrochemical processes such as electroplating and electrowinning. It is also important since it usually relates to wall-to-bed heat transfer. However, reported works on liquid-wall mass transfer in gas–liquid–solid fluidized beds are found to be scarce [3–7].

In many situations of practical importance, flow past solid objects is encountered. Various theoretical and practical aspects of cross-flow had been discussed by Zukauskas [8]. Flow past a single tube, flow past banks of tubes are most common applications found in heat exchangers, reactors, air crafts and space vehicles. Mass transfer applications are found in dissolution, sublimation and electrochemical systems. The heat and mass transfer rates are considerably influenced by the flow regime around the tube. The flow pattern around a tube in a tube bank is greatly influenced by the presence of other tubes. Flow past tube banks is a complex problem of utmost theoretical and practical interest.

In the present investigation, the effects of liquid and gas superficial velocities, particle size, and bed porosity on the liquid-wall mass transfer rates in gas–liquid–solid fluidized beds of inert gas nitrogen and inert particles in cross-flow are investigated. The correlation for the liquid-wall mass transfer coefficient is developed on the basis of Coulburn j-factor approach.

2. Experimental apparatus and procedure

Fig. 1 shows a schematic diagram of the experimental setup for measuring the liquid-wall mass transfer coefficient. The main experimental unit composed of three sections in series; an entrance copper calming section (44.5 mm dia × 1000 mm long) filled with 12.5 mm diameter raschig rings to stabilize flow, a perspex test section of the same i.d. of 800 mm long followed by an exit calming section of same i.d. of 270 mm long.

The test section for cross-flow studies was made out of the perspex tube cut into two halves to facilitate the electrode holder to be paced in line with the perspex column by means of flanges. The electrode holder consisted of two ebonite plates of 6 mm thick with a central hole of 44.5 mm. The electrode is placed in between the two ebonite plates. Two grooves were made for holding the studs of the electrode. In order to prevent leakage, neoprene packing is provided between the two ebonite plates. An insulated copper wire was connected to the stud of the electrode at one end and was carefully drawn out through the packing for electrical measurements. The test section is connected to the entrance calming section by flange arrangement at one end and to the perspex column at the other end by the same arrangement. A stainless steel screen mesh dividing the calming section and the test section served as a distributor and supported the fluidizing bed.

The test electrodes for cross-flow studies were made of copper in five different diameters, viz., 3, 5, 7.5, 10 and 12.5 mm. Limiting current measurement was facilitated by a circuit consisted of an electronic potentiometer, an ammeter, a 2 V battery and a rheostat. A commutator in the circuit facilitated the reversal of applied potential for obtaining data for oxidation and reduction under the same conditions.

The liquid-wall mass transfer coefficients (k_L) were determined using the following equation [9] where i_L is the limiting current.

$$k_L = \frac{i_L}{zFAC_0} \quad (1)$$

The electrolyte solution was an equimolal mixture (0.01 M) of potassium ferricyanide and ferrocyanide with an excess indifferent electrolyte of 0.5 M NaOH. The concentrations of ferrocyanide and ferricyanide ions were analyzed for each run. The ferrocyanide ion concentration was determined by permanganometry, ferricyanide ion concentration by iodometry. In all the runs the ferrocyanide and ferricyanide ion concentrations were maintained at 0.01 M by periodical makeup. The physicochemical properties and diffusivities of electrolyte were taken from Lin et al. [9] data.

About 80 l of electrolyte was pumped from 100 l storage tank passed through the column and was recycled to the feed storage tank. The flow of electrolyte to the column was measured by calibrated rotameters and controlled manually through globe valves. The top of the storage tank was covered with an ebonite sheet. The electrolyte was deaerated and saturated with

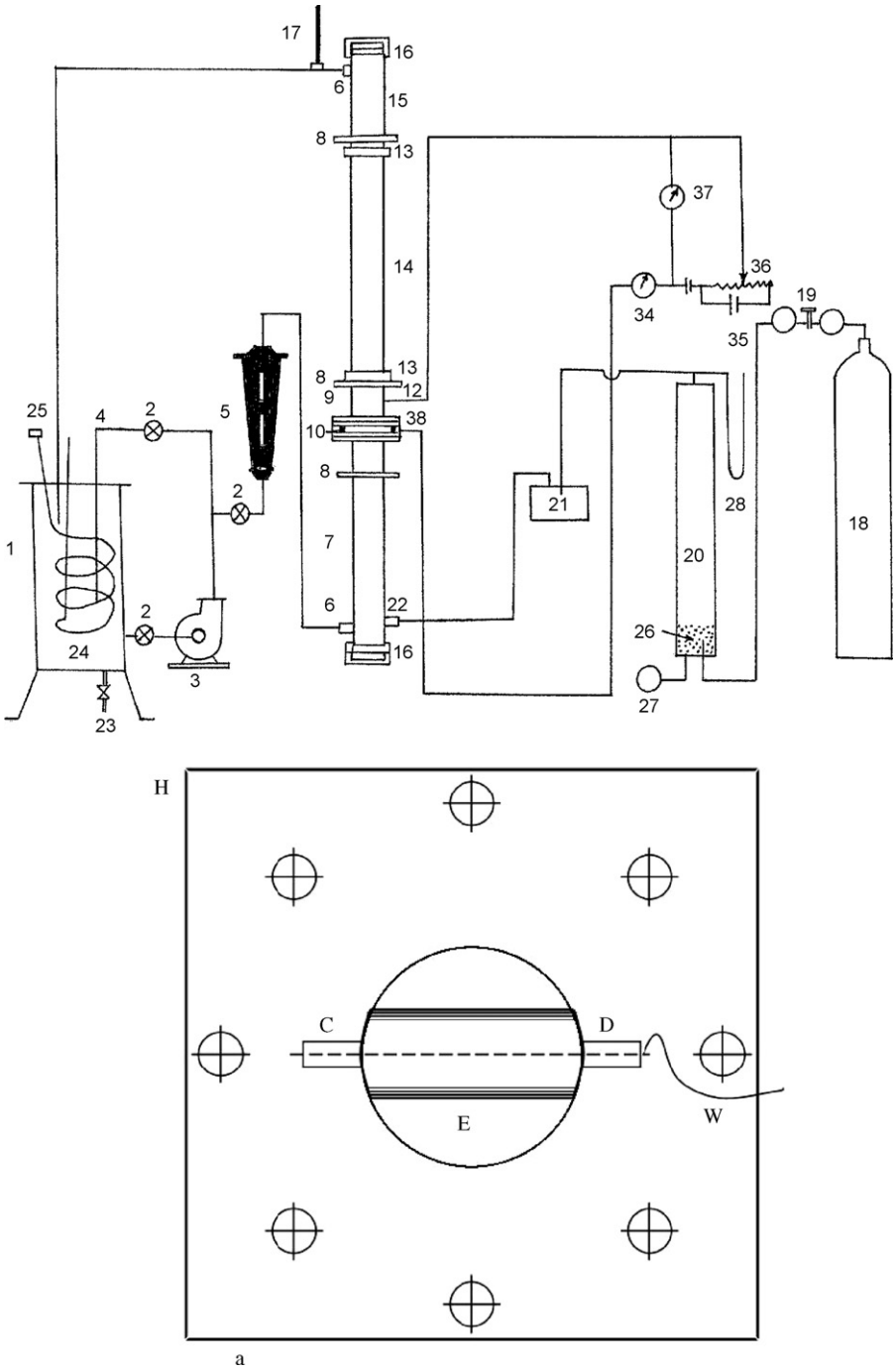

Fig. 1. Experimental set-up. (1) Storage tank, (2) control valves, (3) pump, (4) by-pass line, (5) rotameter, (6) inlet and outlet pipe connections, (7) calming section, (8) flanges, (9) test section, (10) inner test electrode, (11) capillary gland, (12) wall electrode, (13) glands, (14) perspex column, (15) exit calming section, (16) end glands, (17) thermometer, (18) nitrogen gas cylinder, (19) pressure regulator, (20) soap bubble meter, (21) soap separator, (22) gas inlet, (23) nozzle gland for nitrogen inlet, (24) coiled copper tube, (25) dummy plug, (26) soap solution, (27) suction bulb, (28) mercury manometer, (29) stop cock, (30) KCl solution bulb, (31) KCl solution, (32) calomel electrode, (33) potentiometer, (34) ammeter, (35) battery, (36) rheostat, (37) voltmeter, (38) electrode holding flanges. (a) Electrode holder, (C) and (D) grooves for the studs of the electrode; (E) electrode, (H) Hylam flange plate, (W) wire.

nitrogen prior to use. Nitrogen atmosphere was maintained by slow bubbling of nitrogen into the storage tank through the coil provided.

Nitrogen flow rate was measured by using a soap bubble meter. The inlet pressure of nitrogen to the soap bubble meter and the pressure in the soap bubble meter were taken from the pressure gauge and from the mercury manometer, thus maintaining the flow rate of electrolyte constant at various nitrogen gas flow rates.

Initially the equipment was standardized, by checking the reproducibility of literature data. The bed porosity data in liquid–solid fluidized bed were well correlated with Richardson–Zaki equation [10]. The liquid-wall mass transfer data in liquid–solid fluidized beds were in good agreement with

Table 1
Properties of the particles used

S. no.	Particle	Diameter, d_p (mm)	Density, ρ_s (kg/m^3)	Terminal velocity, U_t (mm/s)
1	Glass balls	3.0	2450	230
2	Glass balls	4.1	2500	300
3	Glass balls	6.0	2450	380
4	Glass beads	3.4	2420	260
5	Rock wool shots	1.3	2750	160

Table 2
Range of variables studied

S. no.	Parameter	Range
1	Particle diameter, d_p (mm)	1.3–6.0
2	Particle density, ρ_s (kg/m^3)	2420–2750
3	Electrode diameter, d_e (mm)	3.0–12.5
4	Liquid velocity, U_L (mm/s)	43.0–156.0
5	Gas velocity, U_g (mm/s)	0.0–270.0
6	Bed porosity, ε	0.450–0.822
7	Mass velocity ratio, G_{mr}	0.0–0.006

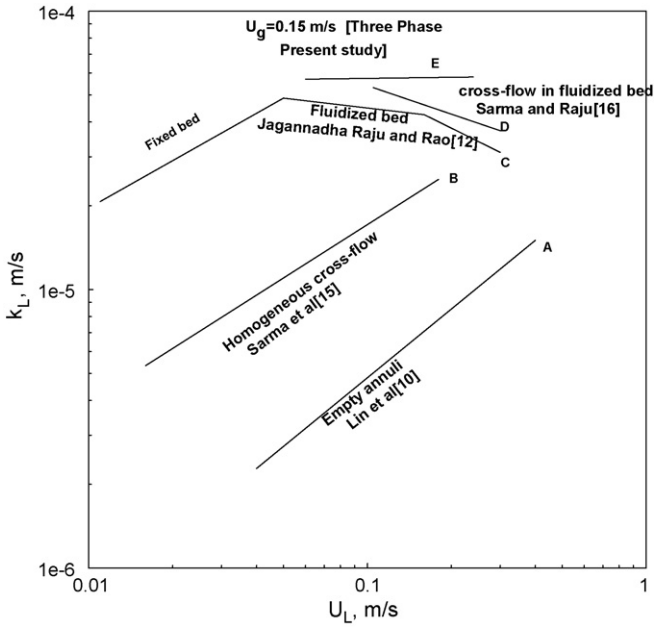

Fig. 2. Augmentaion of k_L with U_L in different flow systems.

Jagannadha Raju and Venkata Rao [11]. The minimum liquid fluidization velocity data in liquid–solid fluidized beds is in accordance with Ergun equation [12]. In three-phase fluidized beds, the solids holdup is determined from bed height measurements and the bed porosity data thus obtained were found to obey the equation of Kim et al. [13]. The gas holdup data were determined from pressure drop measurements and were found to agree with the equation of Soung [14].

Prior to the commencement of each set of experiments, the electrode was cleaned with fine emery paper to remove the corrosion products and other deposits on the surface. For any individual run the temperature was kept constant within ±0.1 °C. The bed materials employed in the present study are given in Table 1. The ranges of variables covered are presented in Table 2.

3. Results and discussion

Fig. 2 gives the data plotted as k_L against liquid velocity U_L for five cases of (i) empty annuli (plot A), (ii) cross-flow of homogeneous fluid (plot B) (iii) heterogeneous two phase fluidization (plot C), (iv) cross-flow in fluidized beds (plot D) and (v) heterogeneous three phase fluidization (plot E). The magnitudes of improvements over empty annuli are shown through plots B, C, D and E. Plot A is the data predicted from the equation of Lin et al. [9] for the case of empty annuli. Plot B is the data predicted from the equation of Bhaskara Sarma et al. [15] for the case of cross-flow with homogeneous fluid. The presence of cross-flow electrode element creates turbulence around itself resulting in increased mass transfer. In case of fluidized beds, the improvements in coefficients at the electrode wall is attributed to the increased turbulence resulting by the convective movement of the solids and greater interstitial velocities. The data of Jagannadha Raju and Venkata Rao [11] for fluidized beds is shown in plot C. In case of cross-flow in fluidized beds the increased velocity although reduces the solids concentration increases the coefficients due to the turbulence generated by its orientation being perpendicular to flow, shown by plot D representing the data of Bhaskara Sarma and Jagannadha Raju [16]. In case of three-phase fluidization the present experimental data were plotted for a gas velocity of $U_g = 150$ mm/s (plot E). Plots B, C and D show that the improvements in the liquid-wall mass transfer coefficients in a two-phase fluidized bed are in the range 8–10-fold over the empty annuli (plot A), while plot E gives augmentation in liquid-wall mass transfer coefficients due to introduction of gas in three-phase fluidized beds is in the range 15–25% over two phase solid–liquid fluidized system. These observations indicated that the introduction of gas is definitely advantageous which caused an additional turbulence resulting in a significant decrease in the thickness of the resistance film to diffusional mass transfer.

3.1. Effect of gas velocity on k_L

The enhancement in the heat and mass transfer rates for a given system can be achieved by overcoming the resistance offered to the concerned transfer process. The fluid film present on the transfer surface is a major component of the resistance. This resistance can be overcome by decreasing the thickness of this surface film. In liquid–solid fluidized beds the solids recirculation process within the bed and their scouring action together result in a decrease in the thickness of the surface film thus contributing to substantial improvement in heat and mass transfer coefficients. The addition of gas flow in the liquid–solid fluidized bed increases the turbulence and intensity of mixing and leads to further augmentation in the heat and mass transfer rates. It may be presumed that the increase in k_L is initially rapid at low U_g and finally tends towards a steady constant value at

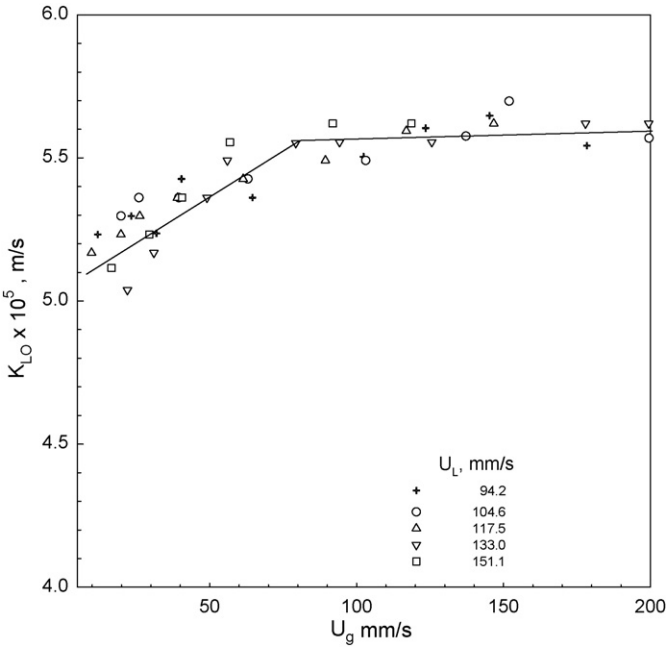

Fig. 3. Variation of K_{LO} with superficial gas velocity U_g for $d_e = 10$ mm, $d_p = 4.1$ mm.

higher values of U_g. Because, further increase in gas velocity could not contribute to scouring action of the solids thereby the fluid film under these conditions remains nearly unaffected. The effect of gas velocity on the liquid-wall mass transfer coefficient in the present study is shown in Fig. 3 at different liquid velocities. It was found that the liquid-wall mass transfer coefficient increased with an increase in gas velocity within the range of present study and reached a plateau. These observations are in agreement with those of Morooka et al. [4] and Yasunishi et al. [5] in their studies on wall-to-bed mass transfer. The particle-to-liquid mass transfer data of Arters and Fan [17] also showed similar trend.

3.2. Effect of liquid velocity on k_L

Interstitial velocity of the continuous liquid phase is further increased due to the introduction of gas in a liquid–solid fluidized bed leading to the vigorous stirring of the bed. The turbulent mixing of the fluid elements is expected to contribute higher augmentation in the liquid-wall mass transfer coefficients at the confining wall which can be attributed to the effective reduction in the boundary layer thickness due to the prevailing tractive shear at the electrode surface. It is anticipated that, initially with increase in liquid velocity, the turbulence increases leading to increase in k_L to a maximum. Further increase in liquid velocity renders the bed leaner, and the interaction between the solids and the reacting surface drastically falls resulting in lower values of k_L. Fig. 4 shows the effect of liquid velocity on k_L for $U_g = 20$, 50 and 150 mm/s. The liquid velocity was varied from minimum fluidization values to values well below the corresponding terminal velocities of the particles employed. The liquid-wall mass transfer coefficient was found to increase with increase in liquid velocity. However, within the range of

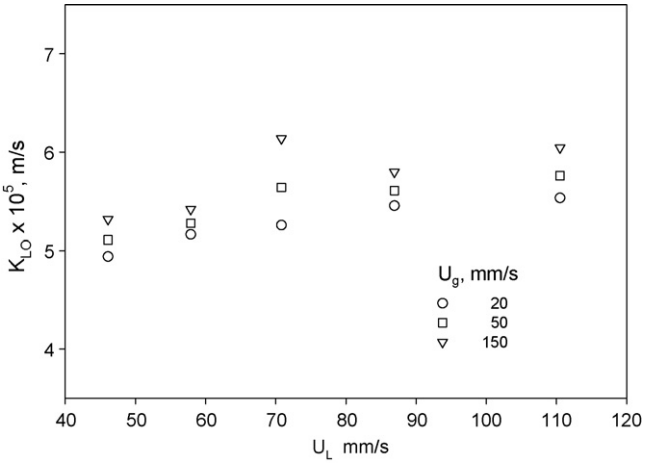

Fig. 4. Variation of K_{LO} with superficial liquid velocity U_L for $d_e = 3$ mm, $d_p = 1.3$ mm.

U_L investigated in the present study, as outlined above a maximum for k_L was not observed. Bhaskara Sarma and Jagannadha Raju [16] reported a decline in mass transfer coefficients at high liquid velocities in their studies on cross-flow in liquid fluidized beds.

3.3. Effect of electrode diameter on k_L

Fig. 5 shows the variation of k_L with U_g for 4.1 mm glass spheres with electrode diameter as parameter. It was found that an increase in electrode diameter decreased the k_L values. In the transverse flow, the velocity is maximum at the maximum cross section of the electrode placed horizontally, or where the area available for flow is minimum. The voidage in the bulk differs entirely from the voidage in and around the horizontal cylindrical electrode. Bhaskara Sarma et al. [15] derived an equation for corrected velocity for cylindrical and elliptical cross-flow elements in homogeneous flow. For the case of cross-flow in fluidized beds, Bhaskra Sarma and Jagannadha Raju [16] obtained

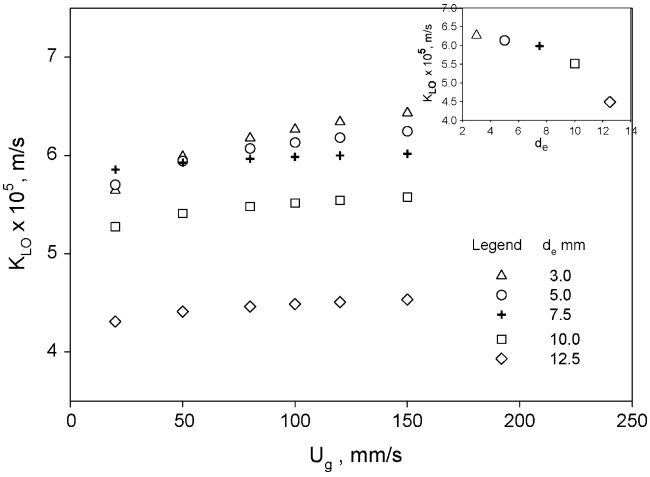

Fig. 5. Variationof K_{LO} with U_g for different electrode diameters d_e for $d_p = 4.1$ mm, $U_L = 100$ mm/s.

corrected bed voidage corresponding to corrected velocity read from the plot of voidage versus liquid velocity. When the corrected liquid velocity at the maximum plane cross-section is higher than the terminal velocity of particles, that results in a particle devoid zone at the maximum diameter plane while the particles remain in a state of fluidization in the forward and rear portions. The situation becomes more and more pronounced as the electrode diameter is increased, consequently a decrease in the liquid-wall mass transfer coefficient was observed. The effect of electrode diameter is also shown in the cross-plot as an inset of Fig. 5. Bhaskara Sarma et al. [15] reported a decrease in the liquid-wall mass transfer coefficient with increase in electrode diameter in cross-flow with homogeneous fluid. Similar observations were reported by Bhaskara Sarma and Jagannadha Raju [16] for cross-flow in liquid fluidized beds and Subba Raju [7] in three-phase fluidized beds.

3.4. Effect of particle diameter on k_L

The earlier studies on batch liquid fluidized beds in cross-flow [16] revealed that the liquid-wall mass transfer coefficients increased with increase in the particle diameter. Convective movement of particles has remarkable effect on augmentation of the liquid-wall mass transfer coefficients by scouring action. Fig. 6 shows the effect of particle diameter on k_L. Two plots A and B obtained as k_L plotted against U_g for each case. Plot A gives the data in the range of $d_p > 4$ mm and similarly plot B gives the data in the range of $d_p < 4$ mm. In three-phase fluidized beds the augmentation in liquid-wall mass transfer coefficients due to an increase in the particle size is marginal consequent to the introduction of gas, which seemed to have masked the particle size effect. The data covering the entire range of particle sizes used in the present study have thus been found to be segregated into two regions, one for $d_p < 4$ mm while the other for $d_p > 4$ mm. Data in plot A showed no parametric effect of particle size greater than 4 mm. Similarly data on smaller particles of $d_p < 4$ mm also showed no parametric effect of particle diameter within that range. However, the coefficients for particles having

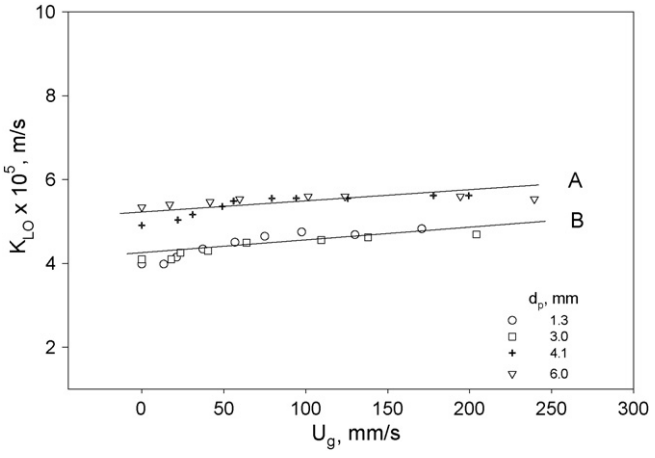

Fig. 6. Variation of K_{LO} with superficial gas velocity U_g. Effect of particle diameter for $U_L = 133$ mm/s and $d_e = 100$ mm.

$d_p < 4$ mm are found to be consistently lower than that of particles of $d_p > 4$ mm. Dhanuka and Stepanek [18] and Nguyen-Tien et al. [19] reported that particle size above 4 mm are more effective to increase mass transfer in three phase fluidized beds. Nikov and Delmas [20] while studying particle-liquid mass transfer in three phase fluidized beds reported that the mass transfer coefficient k_L appears to be approximately independent of the size of the particles. Two ranges are clearly visible; one for $d_p < 4$ mm (plot A) and other for $d_p > 4$ mm (plot B). Hence segregation of the data for the purpose of developing a generalized correlation was done by defining a critical Reynolds number, Re_t, critical based on the terminal velocity of the particle, which was found to be in the present case, 1400. The terminal velocities of the particles were obtained using Richardson and Zaki [10] correlations by extrapolating the liquid velocity for unit bed porosity at constant gas velocity.

3.5. Effect of bed porosity ε on k_L

The expansion of the bed influences the fluidized bed volume and hence the residence time(s) of the different fluid phase(s). The fluidizing solids, besides providing churning action in the column, facilitate the mechanism for increasing the liquid-wall mass transfer. It was presumed that through this mechanism, provided by the scouring action of solids on the wall, the thickness of the boundary layer offering resistance to mass transfer is considerably reduced there by increasing significantly heat and mass flux at the confining wall. Introduction of gas flow into a liquid–solid system is likely to promote turbulence intensity resulting in rigorous mixing of the solids. The intensity of turbulence in any three-phase fluidized bed may be attributed to (i) resistance to the upward fluid flow, (ii) breaking up of bubbles due to the presence of solids and then scattering of the disintegrated bubbles due to the convective movement of the solid particles and (iii) increase in the contacting frequency with the reacting surface. Further, it may be presumed, that the fluidizing solids would interact with the bubble flow, thus, the bigger size bubbles were broken, promoting the efficient dispersion of the bubbles. The flow patterns at the confining wall were considerably changed to the advantage of increased mass or heat flux at the wall. This interacting mechanism could well be represented by fraction of solids (ε_s) or bed porosity (ε) in three-phase fluidized beds and the patterns of flow due to liquid–gas and gas–solid and liquid–solid interactions. The flow patterns get modified with gas flow and solids fraction. At low gas velocities, the gas holdup is lower, and as the gas is passing through the bed of solids, the bubbles coalesce to give rise to large bubbles; at higher gas–liquid flow rates, the movement of particles cause bubble disintegration and scattering which significantly affect the boundary layer structure at the wall. Therefore, effective movement of the particles at optimum bed porosity condition would yield maximum transfer coefficients. The present experimental data on liquid-wall mass transfer coefficient were plotted against bed porosity ε, for a constant $U_L = 162.7$ mm/s and $d_p = 4.1$ mm and shown in Fig. 7. Within the range of ε covered in the present study, k_L increased with increase in ε, reached a maximum at $\varepsilon = 0.75$, remained constant upto $\varepsilon = 0.85$,

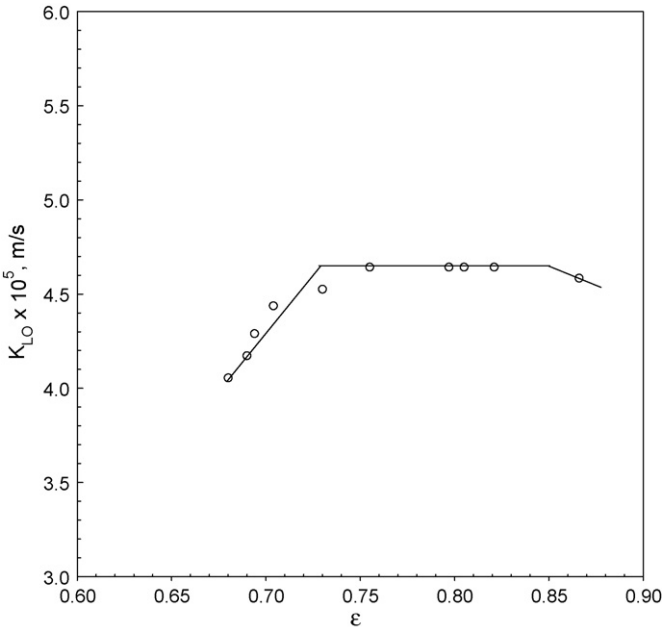

Fig. 7. Effect of bed porosity ε on mass transfer coefficient at constant $U_L = 162.7$ mm/s, $d_p = 4.1$ mm and $d_e = 100$ mm.

then decreased slightly beyond an ε value of 0.85. The studies [11] on liquid-fluidized beds revealed that the liquid-wall mass transfer coefficients beyond an ε value of 0.75 declined. Higher values of liquid-wall mass transfer coefficients were found in three-phase fluidized beds even under rear bed conditions. This may be attributed to the turbulence due to the intense recirculation of the solids resulting from gas flow. Similar trends of the data were observed for all the cases of bed materials used in the present study.

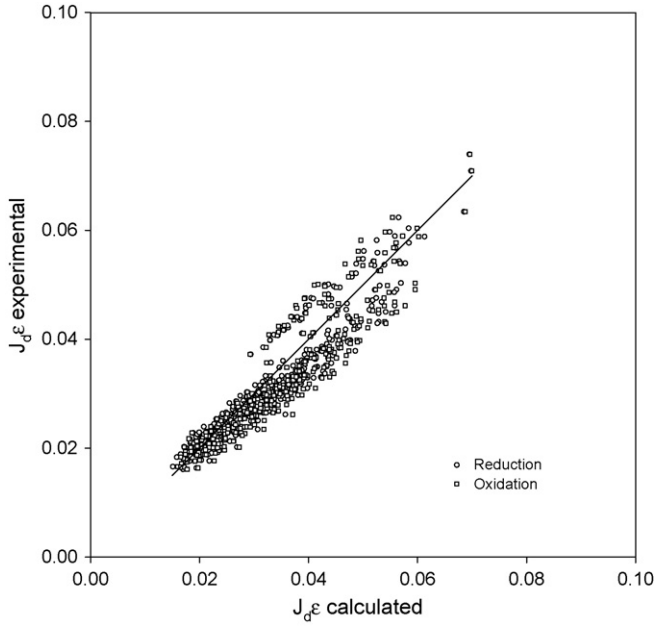

Fig. 8. Correlation graph.

4. Correlations

The entire data on liquid-wall mass transfer coefficient in three-phase fluidized beds with cross-flow of fluid electrolyte have been correlated with Coulburn j_D-factor, void fraction ε, Reynolds number based on electrode diameter Re, Froude number based on gas velocity Fr_g and mass velocity ratio G_{mr}. The following correlations are obtained on regression analysis of the data:

For the case of $d_p < 4$ mm

$$j_D\varepsilon = 1.803 Re^{-0.607} Fr_g^{-1.075} G_{mr}^{1.153} \quad (2)$$

Average deviation = 5.864%. Standard deviation = 7.233%.

For the case of $d_p > 4$ mm

$$j_D\varepsilon = 1.218 Re^{-0.503} Fr_g^{-0.205} G_{mr}^{0.271} \quad (3)$$

Average deviation = 7.972%. Standard deviation = 9.927%.

The comparison between the experimental and calculated $j_D\varepsilon$ data is shown in Fig. 8 for both the cases of oxidation of ferrocyanide and reduction of ferricyanide.

5. Conclusions

1. The k_L values in three-phase beds are upto a maximum of 30% higher than the k_L values of two-phase beds at corresponding liquid velocities.
2. k_L increased with increase in gas velocity and reached a plateau.
3. Within the range of present study it was observed that the k_L increased with increase in liquid velocity.
4. Increase in ε increased k_L upto a value of $\varepsilon = 0.75$ and remained constant upto $\varepsilon = 0.85$. Further increase in ε decreased the mass transfer due to decrease in turbulence caused by decreased solids concentration.
5. The trend of the present data showed two regions with respect to particle diameter, indicating the existence of critical Reynolds number based on terminal velocity.
6. Increase in electrode diameter decreased the mass transfer coefficient.
7. The data were well correlated in terms of Coulburn j_D-factor.

References

[1] L.-S. Fan, Gas-liquid-solid Fluidization Engineering, Butterworths, Stoneham, MA, 1989.
[2] K. SchÜgerl, Chem. Eng. Sci. 52 (1997) 3661–3668.
[3] J.-K. Lee, H.-S. Chun, L.W. Shemilt, J. Chem. Eng. Japan 30 (1997) 246–252.
[4] S. Morooka, K. Kusakabe, Y. Kato, Int. Chem. Eng. 20 (1980) 433–438.
[5] A. Yasunishi, M. Fukuma, K. Muroyama, J. Chem. Eng. Japan 21 (1988) 522–528.
[6] S.D. Kim, Y. Kang, Chem. Eng. Sci. 52 (1997) 3639–3660.
[7] R.V. Subba Raju, Studies on ionic mass transfer in three-phase fluidized beds with cross and annular flow of electrolyte, Ph.D. thesis, Andhra University, Visakhapatnam, 1991.
[8] A. Zukauskas, Heat transfer from tubes in cross-flow, in: Thomas F. Irvine Jr., James P. Hartnett (Eds.), Advances in Heat Transfer, vol. 8, Academic Press, New York, 1972, pp. 93–158.

[9] C.S. Lin, E.B. Denton, N.S. Gaskill, G.L. Putman, Ind. Eng. Chem. 43 (1951) 2136–2143.
[10] J.F. Richardson, W.N. Zaki, Trans. Inst. Chem. Eng. 32 (1954) 35–53.
[11] G.J.V. Jagannadha Raju, C. Venkata Rao, Indian J. Techol. 3 (1967) 201–205.
[12] W.L. McCabe, J.C. Smith, P. Harriot, Unit Operations of Chemical Engineering, fifth ed., McGraw Hill International Editions, Singapore, 1993, pp. 166–167.
[13] S.D. Kim, C.G.J. Baker, M.A. Bergougnou, Can. J. Chem. Eng. 53 (1975) 134–139.
[14] W.Y. Soung, Ind. Eng. Chem. Proc. Des. Dev. 17 (1978) 33.
[15] C. Bhaskara Sarma, T. Gopichand, G.J.V. Jagannadha Raju, Indian J. Technol. 24 (1986) 580–586.
[16] C. Bhaskara Sarma, G.J.V. Jagannadha Raju, Indian J. Technol. 24 (1986) 309–316.
[17] D.C. Arters, L.-S. Fan, Chem. Eng. Sci. 45 (1990) 965–975.
[18] V.R. Dhanuka, J.B. Stepanek, A.I.Ch.E. J. 26 (1980) 1029–1038.
[19] K. Nguyen-Tien, A.N. Patwari, A. Schumpe, W.D. Deckwer, A.I.Ch.E. J. 31 (1985) 194–201.
[20] I. Nikov, H. Delmas, Chem. Eng. Sci. 42 (1987) 1089–1093.